J Mater Sci (2009) 44:2152–2161
DOI 10.1007/s10853-009-3296-z

Ordering and disordering processes in MA and MM intermetallic iron aluminide powders

Josep M. Guilemany · Nuria Cinca · Lluis Casas · Elies Molins

Received: 17 October 2008 / Accepted: 26 January 2009 / Published online: 26 February 2009

Abstract The formation of the FeAl intermetallic compound has been investigated by annealing a mechanically milled powder and a mechanically cryoalloyed powder. First, the morphological transformations that result from both milling processes were analysed, giving special emphasis to the cryoalloyed powder; the evolution of continuous cold welding and fracturing during milling was assessed by means of scanning electron microscopy (SEM). The lattice parameter changes of both powders were then evaluated as a function of milling time using profile fitting and Rietveld analysis of the XRD data. The powder thermal stability was also examined by differential scanning calorimetry (DSC) and the detected transformations were discussed according to the structural changes observed in X-ray temperature-dependent measurements. Furthermore, Mössbauer data has been used to compare the different atom rearrangements, from that of an ideal B2 structure and a typical bcc-Fe type to a disordered A2-solid solution and their temperature-induced ordering processes.

J. M. Guilemany · N. Cinca (✉)
Thermal Spray Centre (CPT), Department de Ciència dels Materials i Enginyeria Metallúrgica, Universitat de Barcelona, Barcelona, Spain
e-mail: nuria.cinca@ub.edu

L. Casas
Unitat de Cristallografia i Mineralogia, Department de Geologia, Universitat Autònoma de Catalunya, Barcelona, Spain

E. Molins
Institut de Ciència de Materials de Barcelona, ICMAB-CSIC, Barcelona, Spain

Introduction

The idea of disordering intermetallic compounds (IMCs) arose from the challenge of improving their formability. The ordered nature of these compounds leads to attractive high-temperature properties such as high strength, increased stiffness and excellent corrosion/oxidation resistance. However, their low ductility at room temperature as well as their fracture toughness have been a barrier to develop applications for many decades. Thus, it was considerably important to find that introducing some disorder in the lattice provides a reliable improvement of these mechanical properties; therefore, many attempts have been focused on this issue. It is also worth mentioning that significant successes have been also achieved by reducing the grain size or by the addition of certain alloying elements. Especially boron additions have been widely studied since the discovery that not only eliminated the brittle behaviour but also converted the material to a highly malleable form by the preferential location of those atoms at the grain boundaries [1–4].

Intermetallics can be disordered either by heavy plastic deformation like ball milling, by irradiation or by rapid solidification (partially, by a quench from high T in the solid state); amongst them, the first one has been considered to be the most effective method. Besides that, milling results in additional benefits, the inherent embrittlement of the alloy is also overcome by reducing the grain size and modifying the crystal structure [5–7].

Mechanical milling (MM) of ordered intermetallics results in one of the following: a solid solution, an amorphous phase or a different ordered phase with a complex crystal structure. From another standpoint, milling can also be regarded as a synthesis route by which the compound is formed from the mixture of elemental powders; this is

usually referred as mechanical alloying (MA). Some works have even used Powder Metallurgy methods to produce oxide reinforced intermetallic powders mainly to improve the mechanical properties at room- and high-temperature [8–11].

Structural order of IMCs is related to the arrangement of atoms and its deviation from an ideal structure (i.e., compositionally pure, with no dislocations or even lattice vibrations). This order can be quantified using the LRO parameter (Eq. 1), which is related to the range within a given atom arrangement keeps its periodicity.

$$\mathrm{LRO} = \frac{r_\alpha - X_\mathrm{A}}{Y_\beta} = \frac{r_\beta - X_\mathrm{B}}{Y_\alpha} \quad (1)$$

where r_α and r_β are the fraction of A sites and B sites occupied by the "right" atoms (atomic occupation), i.e. A atoms and B atoms, respectively, and, X_A and X_B are the fraction of A and B atoms in the alloy. Y_α and Y_β correspond to the fractions of α and β sites [12, 13].

LRO is larger (maximum 1) at low-temperatures and for stoichometric compositions. Actually, there is a particular temperature (critical temperature, T_c) above which disordering becomes inevitable. Such transition has been observed to be either sharp or progressive and therefore T_c can coincide with T_m (melting temperature) of the material or these become disordered much earlier. However, besides this, the concept order can refer to electronic and nuclear spin states. Electronic magnetic moments come from the presence of unpaired electrons; atoms behave as tiny magnets and impart magnetism to the lattice when present in a parallelly ordered state. Such phenomenon leads to the well-known ferromagnetic order. Here again, there is also a characteristic temperature above which materials become magnetically disordered or paramagnetic [14–17]. All these aspects are studied here for the Fe–Al system using several techniques such as X-ray diffraction at different temperatures, differential scanning calorimetry and Mössbauer spectroscopy.

Both MM and MA processes were used, the first to disorder a prealloyed compound and the latter to synthesize alloys from pure iron and aluminium powders. The whole detailed study of those powders stated a basis for the order-disorder transition. Both milling methods possess interesting features in the frame of this study: (a) on one hand, ball-milled Fe40Al, hereby referenced as *FeAl-grade 3*, which is an atomized + mechanically milled (MM) intermetallic compound (with yttria particles dispersed within it in order to keep a fine grain sized microstructure after hot consolidation treatments [18–20]) and, (b) on the other hand, the cryomilling of Fe and Al powders, hereby referenced as *FeAl-cryo*, was a kind of MA process. Cryomilling results in a better thermal stability because of the formation of nitrides [21]. Thus, by both paths grain growth is reduced; it is worth noting that cryomilling is a new method which is opening new expectations. Once both powders have been produced, these will serve to be sprayed by using cold-spray technologies and thus form coatings without the influence of any oxidation.

Experimental procedure

In order to study the disordering process induced by MM, the commercial *FeAl grade 3* powder (nominal composition Fe–40Al–0.05Zr (at.%) + 50 ppm B + 1 wt% Y_2O_3) supplied by CEA, was investigated. It was supplied as-milled but some unmilled powder was provided for their comparison. In contrast, the MA route was studied starting from a blend of pure elements with a composition Fe25 wt%Al (*FeAl-cryo*). This mixture was mechanically alloyed in a modified Union Process attritor with continuous flux of liquid nitrogen. The balls and vial were made of stainless steel and the ball-to-powder ratio used was 32:1 with a rate of 180 rpm. In order to prevent sticking to the milling media, 0.15 wt% of stearic acid was added to the blend before placing the sample inside the vial. The milling time was set to 3, 6, 9 and 12 h in order to observe the evolution of particle morphology and grain size. The vials were sealed in a glove box under an Ar atmosphere to prevent oxidation during milling.

The samples were examined by Scanning Electron Microscopy; using a JEOL 5510 operated at 20 kV and equipped with an Energy Dispersive Spectroscopy (EDS) for microanalysis.

For phase identification and their evaluation, two different types of X-ray diffraction (XRD) analyses were performed:

- Using a Bragg Brentano $\theta/2\theta$ Siemens D-500 diffractometer with Cu $K\alpha$ radiation, scans from 20° to 120° were recorded with a step size of 0.03° and a step time of 17 s to fit the profiles and undertake Rietveld analysis. The softwares used were XRFIT and FULLPROF, both included in the WinPLOTR graphical tool software package.
  The refinement of the occupational factors enabled the calculation of the long range order parameter according to Eq. 1.
- The temperature-dependent X-ray scans were performed on a Bragg Brentano $\theta/2\theta$ Bruker diffractometer, type D8 Advance, provided with a temperature chamber Anton Paar HTK1200. The recorded $\theta/2\theta$ scans range from 28 to 32° and 42.5 to 47°. This permits to follow the evolution of the most intense superlattice and fundamental lines, (100) and (110), respectively. The temperature range was from 100 °C to 800 °C taking

records for every 100 °C and 50 °C around the temperature peaks observed in the DSC analysis.

The ordering processes were induced by heating in a DSC calorimeter Perkin–Elmer DSC-7 under Ar atmosphere with a constant heating rate of 40 °C/min.

Mössbauer measurements were performed using a conventional transmission Mössbauer spectrometer with a ^{57}Co source diffused into a Rh matrix. Calibration was done using a 25-μm-thick natural iron foil. Spectra were recorded at 300 K and 80 K. The spectra were fitted using Normos program [22]. This technique provides information about Fe oxidation state, iron oxide phase and magnetic structure.

Results

Structural changes upon milling

Morphological evolution of the cryomilled powder is not shown here. However, the alloying process is well represented from cross sections of polished particles (Fig. 1). The higher the milling time, the thinner the iron and aluminium lamellae are. After 3 h of milling, these are well distinguished by the different grey contrasts and they become more uniform when fracturing and cold-welding phenomena become balanced. Nevertheless, the homogeneity never reaches the levels exhibited by the *FeAl-grade 3* sample both as-atomised or after MM (Fig. 2).

Figure 3a shows the XRD patterns of *FeAl-grade 3* sample (as-prepared (atomised) and after MM), whereas Fig. 3b shows the cryomilled powder (i.e., MA) at different milling times. Comparing the atomised with the subsequently milled powder, it is apparent that the milling process induces a peak shift towards lower angles as well as a noticeable broadening of these peaks. On the other hand, the Fe–Al blend milled under cryogenic conditions (*FeAl-cryo*), exhibits a progressive disappearance of the Al peaks, while the Fe peaks become asymmetric. The appearance of the second phase identified as a solid solution only must be only assigned to the spectra milled for more than 3 h because at 3 h Al and Fe peaks are still visible and non-asymmetric.

The evolution of the interatomic distances with the milling time was studied for the experimental *FeAl-cryo*

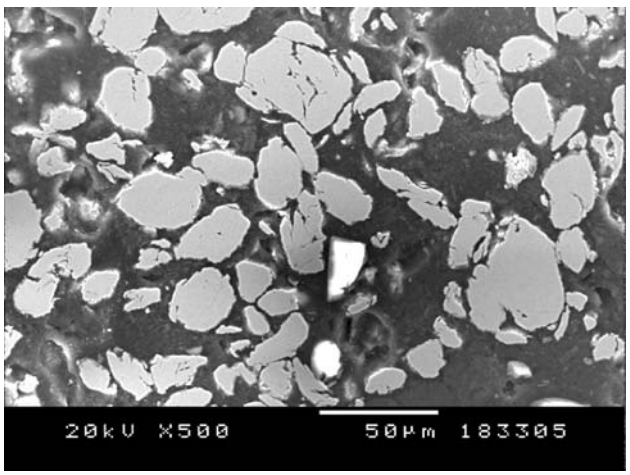

Fig. 2 Cross section of ball-milled powder

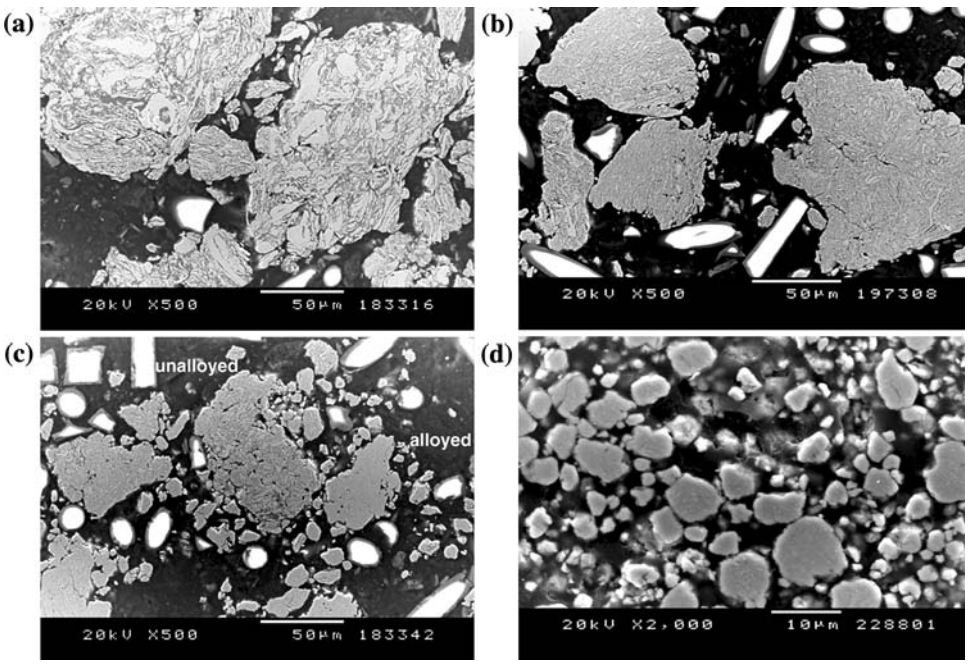

Fig. 1 Cross sections of cryomilled powder at different milling times: **a** 3 h, **b** 6 h, **c** 9 h and **d** 12 h

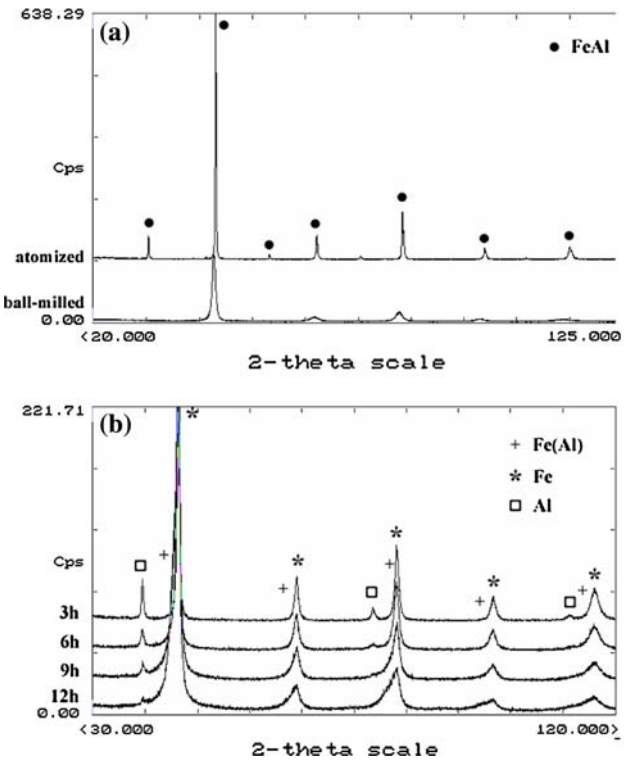

Fig. 3 X-ray scans: **a** atomised and ball-milled powder, **b** cryomilled powder at different milling times

powder by means of a profile fitting methodology and the Rietveld method, as well as for the as-atomised and ball-milled *FeAl-grade 3* powder. Regarding the cryomilled powder (*FeAl-cryo*), it is observed that the iron lattice parameter undergoes a slight and progressive expansion as the new alloy phase Fe(Al) is formed (Fig. 4); the same phenomenon is observed in the *FeAl-grade 3* powder, being the starting value of the lattice parameter 2.89_6 Å (for the atomised sample) and 2.92_1 Å (for the as-ball-milled).

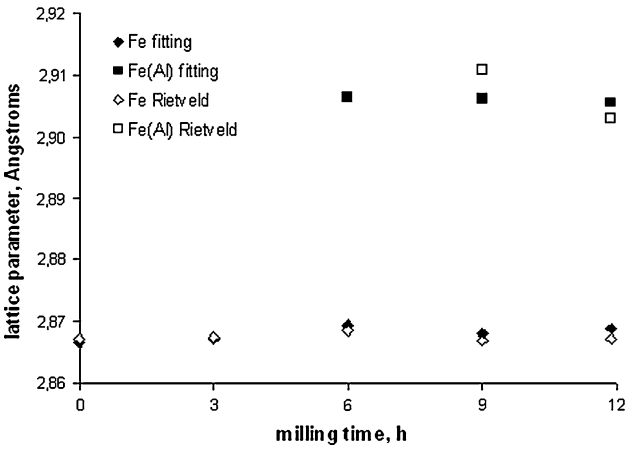

Fig. 4 Refined lattice parameters from XRD data of the cryomilled powder versus milling time

The Mössbauer spectra and the basic parameters of *FeAl-grade 3* and *FeAl-cryo* samples are presented in Fig. 5 and Table 1 respectively. Both spectra are fitted with two components: the minor one consists of a paramagnetic doublet, which is related to Fe atoms introduced in a site surrounded mainly by Al atoms. The other component is a dominant magnetically ordered phase but appears significantly different in both samples. In the *FeAl-grade 3* sample this magnetically ordered phase is not homogeneous and exhibits a very broad distribution of hyperfine fields (see Fig. 5a, inset on the right), whereas in the *FeAl-cryo* sample the magnetically ordered phase appears to be similar to pure Fe although the hyperfine field has been slightly reduced. *FeAl-cryo* sample comes from a blend of pure powders and thus, before any milling, the Mössbauer spectrum shows already a magnetic component, i.e., the 33 T Fe sextet. *FeAl-grade 3* sample instead, comes from a prealloyed product which is paramagnetic and thus shows a magnetically non-ordered Mössbauer spectrum (see Fig. 5a, inset on the left); the magnetically heterogeneous but ordered phase that forms after milling is due to strain-induced ferromagnetism [23, 24]. Low-temperature spectra (at 80 K) appear to be similar to those recorded at 300 K limiting the relevance of dynamic effects such as superparamagnetism. Alloys with even more than 50 at.%Al have shown a ferromagnetic behaviour as result of incompleted milling; a rapid grain refinement occurs leading to a metastable Fe–Al solid solution [25, 26].

Structural changes upon heating

Figure 6 shows the thermal responses of both powders. The ball-milled powder (*FeAl-grade 3*) exhibits an exothermal peak around 200 °C, while cryomilled samples (*FeAl-cryo*) show two different peaks indicating that two exothermic processes are taking place at higher temperatures. Increasing milling time, the energy released by these processes decreases, reaching almost zero at 12 h. Table 2 shows the peak temperatures and Table 3 presents the energies released. Second heating runs were performed on each sample without removing it from the calorimeter and no peaks were detected proving the irreversibility of the observed transitions.

XRD patterns of both powders upon temperature were recorded in order to discern the structural changes. Figures 7 and 8 correspond to the evolution of (100) and (110) lines for *FeAl-grade 3* and *FeAl-cryo*, respectively. It is seen that heating produces the appearance of the superlattice B2 line (100) in both cases. With regard to the fundamental line (110), the *FeAl-grade 3* sample displays a shift to lower angles, whereas the *FeAl-cryo* sample shows a bit more complicated behaviour: the asymmetric peak observed at room temperature results in two narrower but

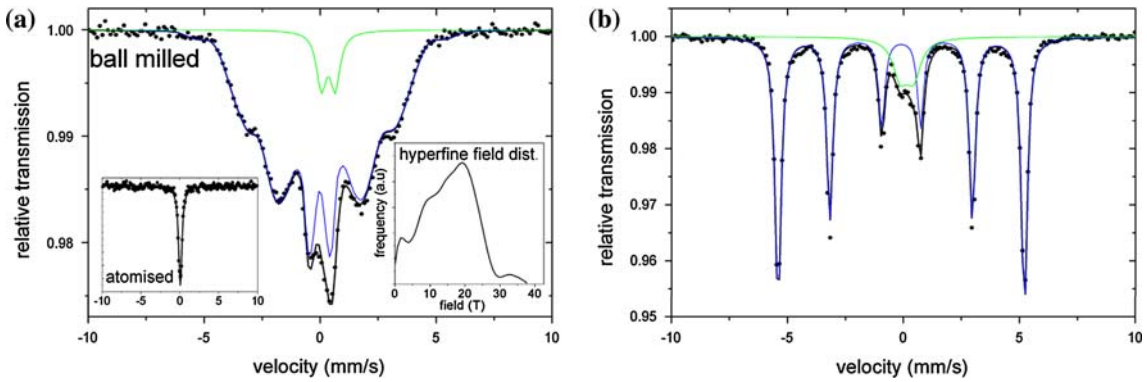

Fig. 5 Mössbauer spectra recorded at 300 K of the starting products: **a** *FeAl-grade 3* (inset as atomised); **b** *FeAl-cryo*

Table 1 Mössbauer parameters of ball-milled and cryomilled powders: linewidth (Γ), isomer shift (δ), quadrupole splitting (Δ), quadrupole shift (2ε), hyperfine field (B_{hf}) and relative subspectral area, % phase

	Subspectrum	Γ (mm/s)	δ_{Fe} (mm/s)	Δ or 2ε (mm/s)	B_{hf} (T)	%
Ball-milled	Sextet	–	0.11(1)	0.04(2)	[a]	93
	Doblet	0.50(8)	0.46(3)	0.59(4)	–	7
Cryomilled	Sextet	0.32(1)	0.01(1)	0.00(1)	32.87(1)	86
	Doblet	0.76(6)	0.25(2)	0.57(3)	–	14

[a] Wide hypefine field distribution with a maximum at 19.2 T

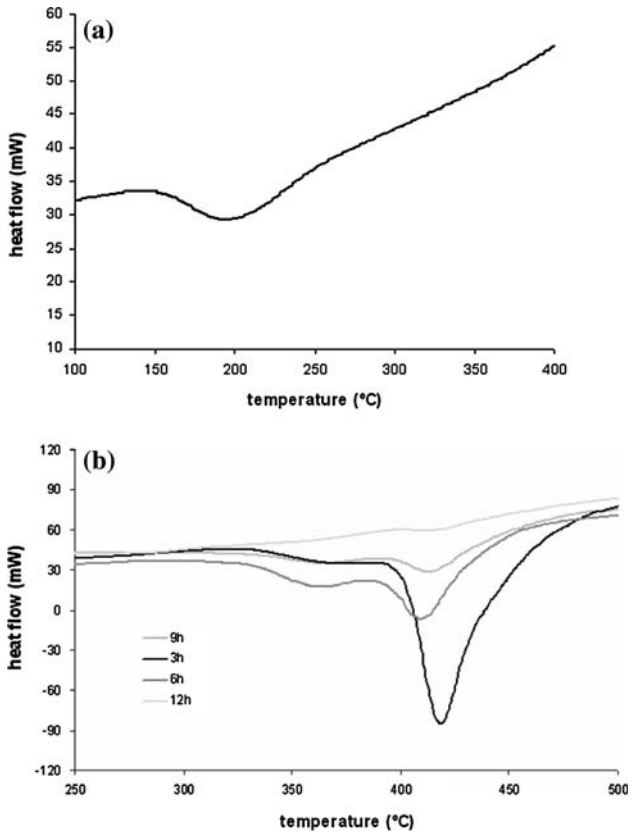

Fig. 6 DSC graphics of the (**a**) ball-milled and (**b**) cryo-milled samples

Table 2 Peak temperatures found in DSC experiments

	Ball-milled	Cryomilled			
		3 h	6 h	9 h	12 h
1r peak, °C	200.8	373.7	362.6	362.6	–
2n peak, °C	–	418.8	409.5	415.5	416.7

Table 3 Peak area of the more intense peak in DSC experiments

	Ball-milled	Cryomilled			
		3 h	6 h	9 h	12 h
Peak area (J/g)	−29.40	−330.47	−210.12	−114.43	−7.37

still overlapped peaks at 350 °C. They become sharper and exchange their relative intensities from 400 to 450 °C, that corresponding to the Fe phase decrease over a Fe(Al) increase. Above 450 °C, the peak assigned to Fe (that at higher angles) disappears and the remaining peak moves slightly to lower angles. Comparing the XRD profile of the atomised powder to that of the ball-milled and subsequently annealed at 700 °C, it is seen that, both show the fundamental and superlattice peaks located at the same positions but the annealed sample exhibits broader peaks.

In Fig. 9, LRO and lattice parameters are plotted against annealing temperature. The *FeAl-grade 3* samples

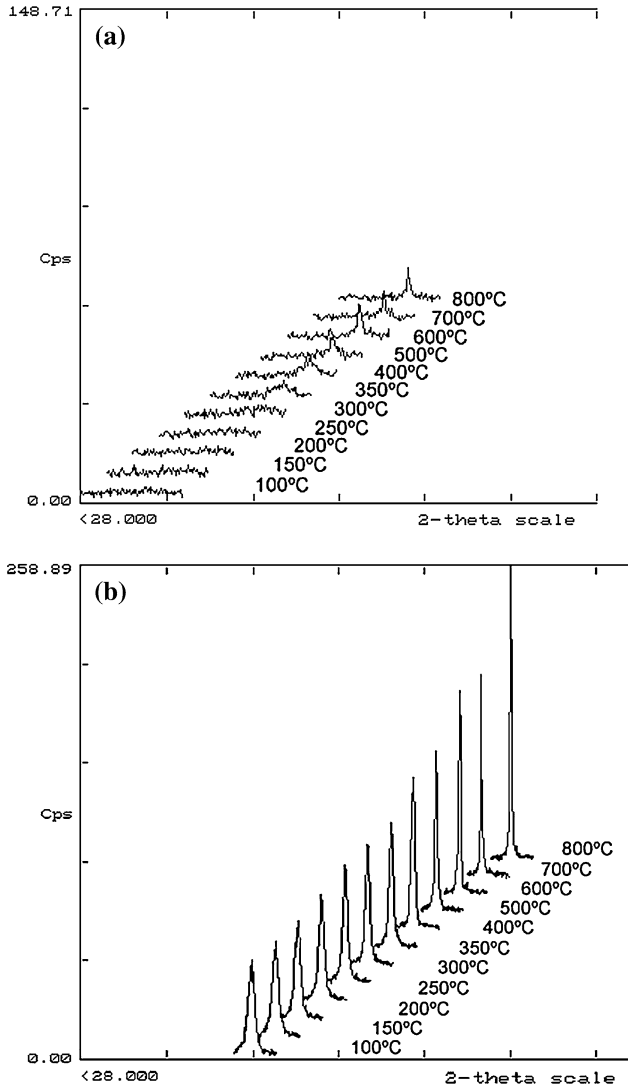

Fig. 7 XRD evolution of the ball-milled powder upon temperature: **a** (100) peak; **b** (110) peak

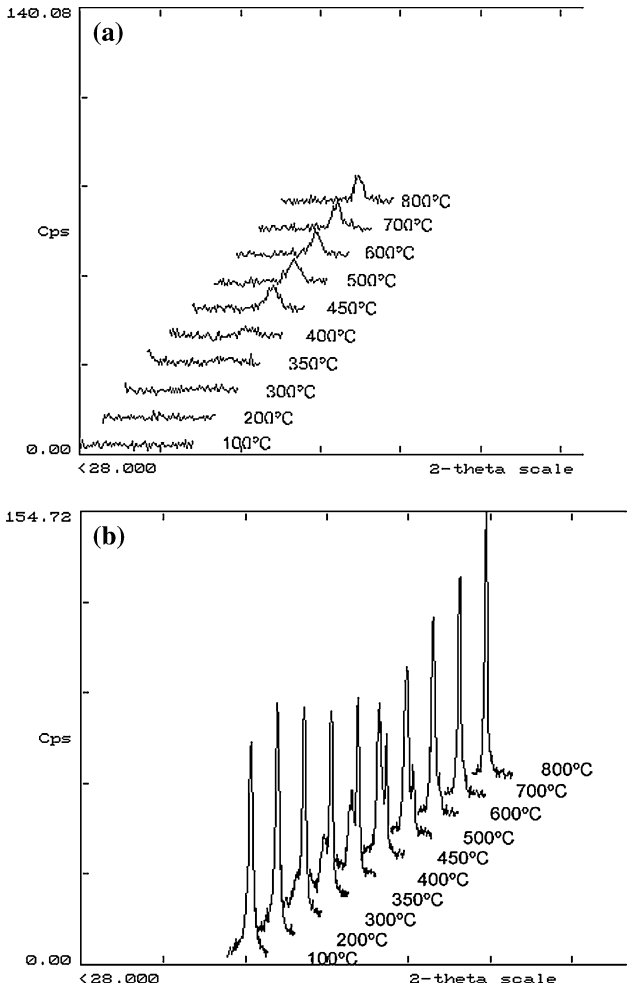

Fig. 8 XRD evolution of the cryomilled powder upon temperature: **a** (100) peak; **b** (110) peak

(as-atomised and after MM) present a decrease of the distance between neighbouring atoms correlated to a rise of the LRO value. For the *FeAl-cryo* powder the same tendency is observed at 500 and 700 °C; at 300 °C the alloys had not been ordered yet, so the calculation is not presented; the values are referred to the 9 h-annealed powder because it is the one which has the optimum particle size for posterior spraying.

Thermally induced changes can also be followed by Mössbauer spectroscopy, see Fig. 10 and Table 4. Upon annealing, milled *FeAl-grade 3* powder loses magnetic ordering and recovers the initial paramagnetic state (Fig. 10a), this would correlate with the return to the previous structurally ordered alloy. *FeAl-cryo* powder also loses progressively the magnetically ordered phase that transforms into a paramagnetic phase, after annealing at 700 °C the magnetic sextet has apparently completely disappeared. However, some magnetism remains since the powder reacts to the presence of a permanent magnet.

Low-temperature measurements (see Fig. 10 insets) reveal that some magnetic ordering is still present, even after annealing at 700 °C, though with different features: *FeAl-grade 3* sample shows a wider peak with respect to the room temperature singlet and *FeAl-cryo* powder reveal the presence of a significant amount of a Fe-rich phase phase (with a hyperfield of around 32 T), which is actually at room temperature.

Discussion

A MA process consists of a continuous deformation-cold welding-fracturing process. According to the morphological changes, the different stages can be described by the following sequence:

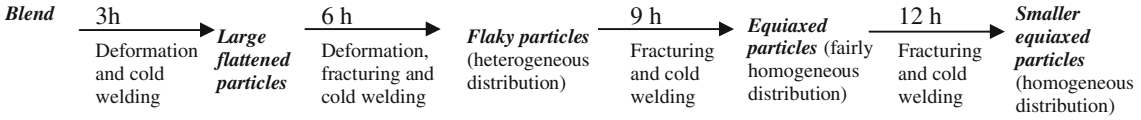

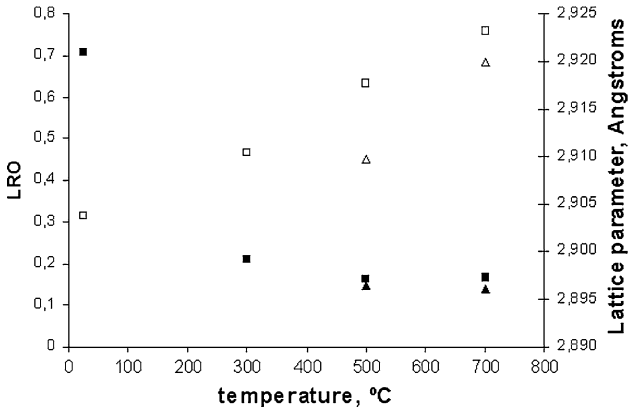

Fig. 9 Lattice parameter (*full*) and LRO (*empty*) versus temperature: (*squares*) *FeAl-grade 3* (MM) powder, (*triangles*) *FeAl-cryo* (MA) powder

Such evolution was observed for the *FeAl-cryo* sample. The less heterogeneity upon milling indicates the evolution of the alloying mechanism. This is associated to the diffusivity of Al atoms into Fe lattice due to the high-temperature reached on milling. The major research carried out on FeAl holds the simple theory that its formation comes from diffusion processes but it can be actually associated to a microscale layers welding. The temperature rise upon milling can be above that of the crystallization point of the quasicrystalline phase produced and therefore an equilibrium intermetallic phase forms under this condition of milling [5]. Few even claim a possible melting of aluminium as a mechanism for FeAl formation [27]. Actually, NiAl has been synthesized through a combustion reaction during milling, but what supports those results is the fact that the ordering energy of NiAl is almost three

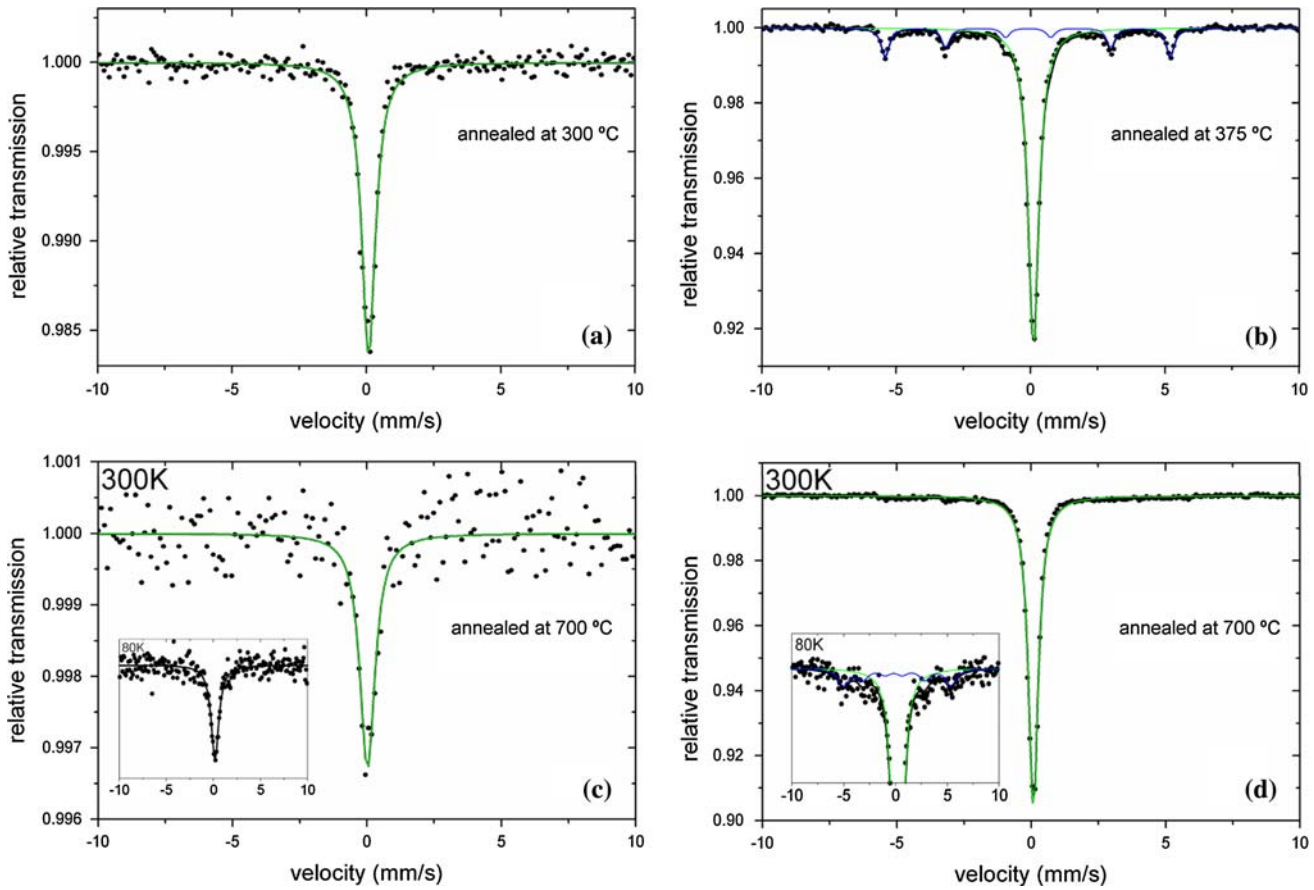

Fig. 10 Mössbauer spectra of the annealed samples for 10 min: **a** *FeAl-grade 3* annealed at 300 °C and **c** 700 °C; **b** *FeAl-cryo* annealed at 375 °C and **d** 700 °C, recorded at 300 K (insets at 80 K)

Table 4 Mössbauer parameters of annealed ball-milled and cryomilled powders: linewidth (Γ), isomer shift (δ), quadrupole splitting (Δ), quadrupole shift (2ε), hyperfine field B_{hf} and relative subspectral area, % phase

Sample	at. (°C)	mt (K)	Sub-spectrum	Γ (mm/s)	δ_{Fe} (mm/s)	$\Delta/2\varepsilon$ (mm/s)	B_{hf} (T)	%
FeAl-grade 3	300	300		0.62(3)	0.19(1)	–	–	100
		80		1.04(4)	0.31(1)	–	–	100
	700	300		0.67(13)	0.12(4)	–	–	100
		80		1.01(9)	0.27(4)	–	–	100
FeAl-cryo	375	300	Singlet	0.48(1)	0.21(1)	–	–	79
			Sextet	0.35(5)	0.00(10)	−0.02(26)	32.85(7)	21
		80	Singlet	0.52(1)	0.33(1)	–	–	76
			Sextet	0.43(5)	0.11(2)	0.01(3)	33.63(8)	24
	700	300	Singlet	0.44(1)	0.19(1)	–	–	92
			Sextet	1.01(15)	0.56(9)	−0.47(12)	32.84(40)	8
		80	Singlet	0.52(1)	0.31(1)	–	–	86
			Sextet	1.25(50)	0.09(10)	0.33(14)	32.17(55)	14

times higher than that of FeAl [28]. In the present case, it could have been difficult to accomplish the stoichiometry even at longer milling times; cryogenic conditions reduce the additional energy contribution supplied by repeated collisions between particles and balls. X-ray and Mössbauer data assert the previous comments. The appearance of low-intensity broad peaks at slightly lower angles than the Fe lines (actually, to some extend, they overlap) reveal the presence of a solid solution, Fe(Al). This new phase has the same bcc structure as α-Fe but with a slightly larger unit cell parameter, which has already been assessed by peak fitting profiles and refinement methods such as Rietveld. The lattice is distorsioned by the introduction of the new Al atoms with larger atomic radius. However, some difficulties arise to determine the exact nature of the new phase: on one hand the assumption that Al atoms do not play a significant role (most of them lie in the same position as those of Fe), on the other hand the deconvolution of overlapped Fe and Fe(Al) lines is a difficult task, the broadening of the XRD peaks during MA may hinder a clear identification of the phases. Mössbauer spectra indicate that the interdiffusion (of Al in the Fe lattice, and Fe atoms in the Al structure) is limited. Although, as it will be commented later, this interdiffusion is greatly reached upon annealing.

As far as the atomised + milled powder is concerned (i.e., *FeAl-grade 3* powder) the morphological evolution from the atomised state to the as-milled upon milling time is not reported because the powder was supplied in its milled state. As a small atomised powder was provided, one can see that the larger lattice parameter compared to that of as-atomised, points out the lower degree of order as a result of the heavy plastic deformation. Most works about B2-ball-milled intermetallic phases have also yielded a disordered A2 structure, commonly with a nanocrystalline structure [27, 29–33]. However, some studies report a transition from crystalline to a completely amorphous state [34, 35] or a reduction of the order degree (related to the particle nanosize) but keeping an ordered nanostructure [6, 36, 37].

Mössbauer spectra reveal the appearance of a strain-induced ferromagnetism [38, 39], not present in the cryomilled sample. It is also worth quoting the role of the grain size and microstrain introduced by such processes [40].

FeAl, as well as Ni_3Al, NiAl, and TiAl, is one of those permanently ordered alloys which show LRO right up to the melting point with a critical temperature $T > T_m$; they can only be disordered by special procedures like irradiation or milling. The two powders studied here possess a disordered structure as a result of milling: one, because the stoichometry is not reached and, the other because, despite having a near stoichiometric composition, a disordering treatment has been carried out. Thus, the evaluation of annealed samples adds extra evidence to the actual production of disordering and is intended to understand both recovering processes until attainment of complete ordering again. On heating both samples, reordering was observed as an exothermic process over a wide range of temperatures. The transition associated to the calorimetric tests of the prealloyed powder (*FeAl-grade 3*) was attributed to the ordering process. Other authors have also reported more complex DSC profiles depending on the milling times. The peak at approximately 200 °C is also common and broad tails are observed at higher temperatures as result of defect recovering and possible grain growth [36, 41–44]; this is as also seen in the present work as the sharpening of lines.

Previous comments are complemented and confirmed by the results obtained by XRD verus temperature. First, XRD reveals the appearance of superlattice lines and a lattice contraction, returning to those values of the unmilled powder. However, the broadening of the peaks even after

annealing indicates that the grain size and microstrain effects are not the same as for the atomised powder.

The disordered arrangement is a metastable state highly strained; thermal energy promotes diffusion, which induces Fe and Al atoms to occupy their most energetically favourable positions. Additionally, the release of strain results in the loss of ferromagnetism because the effect of neighbouring Fe atoms in a B2-structure is not as strong as in a disordered structure. The order parameter approach, which depends directly on the atomic occupation as seen in Eq. 1, demonstrates a progressive increase of LRO. However, even at 700 °C the maximum order of 0.8 for the composition of 40%at. Al is not reached. The explanation given for such phenomenon can be discussed as follows: the perfect order of a crystalline structure only exists at very low-temperatures; over heating, thermal vibration becomes a competitive process. In addition, the present powder is not the exact 50:50 composition, this is why LRO = 1 is not accomplished. Moreover, annealing processes at the same temperatures for longer times (1 h) revealed a decrease in LRO, thus highlighting the effect of temperature against the formation of the B2 lattice. Mössbauer spectra show only a singlet indicating a non-magnetically ordered and highly symmetric site. Therefore, the structural order results in a single phase without magnetic ordering.

The ordering process in the cryomilled powder is a bit more complicated because of the starting Fe + Al mixture was that of the 50:50 stoichiometry but this was not reached after milling. This was not accomplished due to the cryogenic media temperatures as commented before. Then, heating involves two processes: an input energy for alloying and then ordering. Other authors [45, 46] also observed two different peaks for calorimetric traces, which move to lower temperatures on increasing the milling time and become negligible for the longest milling times. The major energy released in the first peak for the least milled samples agrees with the assumption that this is related to the alloying formation: after 3 h of milling, diffusion processes have not had time to take place; iron and aluminium still exist in their elemental form as a layered structure within the particles. As milling continues, these lamellas become thinner and thinner as seen from cross-sections, but it is even difficult to believe that these are thin enough to permit atoms to exchange. Hence, as Mössbauer spectra clearly show, heating is needed to produce the homogenisation of the alloy composition. Once the stoichometry is reached, the minimum free energy state corresponds to that of a 3-D periodic arrangement, this is the B2 superlattice. Krasnowski et al. [29], who observed three instead of two overlapped peaks, have discussed their transformations according to the suppositions made by Morris-Muñoz [7]. They concluded that up to 450 °C, only alloying and ordering take place, whereas above such temperature, the exothermic processes are attributed to the loss of defects, recrystallization and grain growth. Then, as far as *FeAl-cryo* powder is concerned, apart from the transformation discussed for *FeAl-grade 3*, the alloying process has to be also taken into consideration. This causes that higher temperatures be needed to perform the whole transformation.

From XRD patterns, such transition is clearly illustrated: the iron-rich phase coexists for a certain temperature range with Fe(Al) and, after its disappearance, the later one transforms progressively into FeAl. The LRO and Δa point out a shift of the solid solution lattice parameters towards those of the ordered lattice. Mössbauer confirms the decrease of the Fe rich phase (seen as the decrease of the area of the magnetic sextet up to practically zero, see Fig. 10b) and the interdiffusion of Fe and Al atoms in a highly symmetric environment and therefore similar to the situation encountered for *FeAl-grade 3* powder also after application of thermal treatments.

Conclusions

The present work reports the changes on ordering-disordering the lattice of iron aluminide powders obtained through different milling techniques with different purposes as well.

With regard to *FeAl-grade 3* powder:

- When milling the atomised Fe40 at.%Al powder, the structure is rearranged in the way that iron and aluminium atoms are no more surrounded by unlike neighbours. Consequently, the B2 framework is partially destroyed. This change is noticed by the shift of the lattice parameter and more evident, by the evolution of a singlet indicating a paramagnetic structure, into a hyperfine distribution in Mössbauer spectra.
- Milling also produces a decrease of grain size and introduces a high strain according to the broader XRD peaks. Both, ordering and recovering processes are encountered when the samples are annealed.
- After annealing at 700 °C, the lattice parameter decrease is about 0.8%, the same order as the increase after milling the atomised powder. The hyperfine field distribution collapses again into a paramagnetic structure similar to the observed for the atomised powder.

As far as *FeAl-cryo* powder is concerned:

- In the as-mechanically milled powder, a lattice expansion is observed as a result of disordering of the lattice. Here, however, there is an expansion of the iron lattice because of the introduction of aluminium atoms when the powder mixture is mechanically milled.

A complete alloying is not reached for as-cryomilled powder because of the low-temperature of the synthesis route, which inhibits the diffusion processes. At such temperatures, any heat released would be readily dissipated. Thus, iron clusters keep its ferromagnetic ordering.

- When annealing, the alloying is produced first and the ordering consecutively. A higher energy release is observed in the samples milled for shorter times because more energy is needed to accomplish the intermetallic.
- When the cryomilled powder is annealed, the lattice parameter returns to that of a typical B2 structure. Ferromagnetic clusters become smaller as they diffuse into Al and they only appear as relicts after annealing at 700 °C.

A further interesting step could be the study of the role that dispersed particles (e.g., yttria and nitrides) play in each case in connection with thermal stability and grain growth. Many works report that this is really a difficult task but it would possibly add on the understanding on the nanocrystallization process and its temperature dependent effect.

Acknowledgements The Thermal Spray Center would like to thank CEA-CEREM for the kind supply of ODS-Fe40Al powder and N. Cinca wants to specially thank Prof. E. Lavernia's group for the stay in UC Davis to produce the cryomilled powder and X. Alcobé (Serveis Cientificotècnics, UB) for his advices around Rietveld refinements. This work has been supported by the Generalitat de Catalunya project 2005 SGR 00310 and the Ministerio de Educación y Ciencia for the project MAT2006-06025. N. Cinca also wants to acknowledge the Ministerio de Educación y Ciencia for the grant of researcher personnel with reference number AP-2004-2453.

References

1. Rico MM, Greneche JM, Perez GA (2005) J Alloy Compd 398:26
2. Liu CT, George EP, Maziasz PJ, Scneibel JH (1998) Mater Sci Eng A 258:84
3. Pang L, Kumar KS (1998) Mater Sci Eng A 258:161
4. Raulot JM, Fraczkiewicz A, Cordonnier T, Aourag H, Grosdidier T (2008) J Mater Sci 43:3867. doi:10.1007/s10853-007-2338-7
5. Suryanarayana C (2001) Prog Mater Sci 46:1
6. Morris DG, Amils X, Nogués J, Suriñach S, Baró MD, Muñoz-Morris MA (2002) Int J Non-equilib Process 11:379
7. Morris-Muñoz MA, Dodge A, Morris DG (1999) Nanostruct Mater 11(7):873
8. Schicker S, García DE, Gorlov I, Janssen R, Claussen N (1999) J Am Ceram Soc 82(10):2607
9. Akhtar F (2009) Mater Sci Eng A 499:415
10. Hu W, Gottstein G (2002) Mater Sci Eng A 338:313
11. Khodaei M, Enayati MH, Karimzadeh F (2008) J Mater Sci 43:132. doi:10.1007/s10853-007-2123-7
12. Cullity BD (1978) Elements of X-ray diffraction, 2nd edn. Addison-Wesley, USA
13. Porter DA (1981) Phase transformations in metals and alloys, 2nd edn. Van Nostrand Reinhold, New York
14. Rao CNR, Rao KJ (1977) Phase transitions in solids, 1st edn. McGraw-Hill, England
15. Pfeiler W, Sprusil B (2002) Mater Sci Eng A 324:34
16. Argren J (2002) Scripta Mater 46:893
17. Sima V (2004) J Alloys Compd 378:44
18. Ji G, Grosdidier T, Bozzolo N, Launois S (2007) Intermetallics 15:108
19. Arzt E, Behr R, Göhring E, Grahle P, Mason RP (1997) Mater Sci Eng A 234–236:22
20. Muñoz-Morris MA, Garcia Oca C, Morris DG (2003) Acta Mater 51:5187
21. Chung KH, He J, Shin DH, Schoenung JM (2003) Mater Sci Eng A 356:23
22. Brand RA (1987) Nucl Instrum Methods Phys Res B 28:417
23. Apiñaniz E, Garitaonandia JS, Plazaola F (2001) J Non-Cryst Solids 287:302
24. Zeng Q, Baker I (2007) Intermetallics 15:419
25. Sebastian V, Lakshmi N, Venugopalan K (2007) Intermetallics 15:1006
26. Sebastian V, Lakshmi N, Venugopalan K (2007) Mater Lett 61:4635
27. Wolski K, Le Caër G, Delcroix P, Fillit R, Thévenot F, Le Coze J (1996) Mater Sci Eng A 207:97
28. Schröpf H, Kuhrt C, Arzt E, Schultz L (1994) Scripta Metall Mater 30(12):1569
29. Krasnowski M, Grabias A, Kulik T (2006) J Alloys Compd 424(1–2):119
30. Oleszak D, Shingu PH (1994) Mater Sci Eng A 181–182:1217
31. Eelman DA, Dahn JR, MacKay GR, Dunlap RA (1998) J Alloys Compd 266:234
32. Enayati MH, Salehi M (2005) J Mater Sci 40:3933. doi:10.1007/s10853-005-0718-4
33. Varin RA, Bystrzycki J, Calka A (1999) Intermetallics 7:917
34. Huang B, Ishihara KN, Shingu PH (1997) Mater Sci Eng A 231:72
35. Dong YD, Wang W, Liu H, Xiao LKQ, Tong SH, He YZ (1991) Mater Sci Eng A 134:867
36. Shi H, Debo G, Yifang O (2008) J Alloys Compd 455:207
37. Gialanella S (1995) Intermetallics 3:73
38. Wu D, Baker I (2002) Mater Sci Eng A 239–331:334
39. Kiss LF, Kaptas D, Balogh J, Bujdoso L, Gubicza J, Kemeny T, Vincze I (2004) Phys Stat Solidi 201(15):3333
40. Farghalli AM, Yuwei X (2003) Mater Sci Eng A 354:133
41. Meyer M, Mendoza-Zelis L, Sánchez FH (1999) Phys Rev B 60(5):3206
42. Gialanella S, Amils X, Baro MD, Delcroix P, LeCaër G, Lutterotti L, Suriñach S (1998) Acta Mater 46(9):3305
43. Suriñach S, Amils X, Gialanella S, Lutterotti L, Baro MD (1997) Mater Sci Forum 235–238:415
44. Boufenghour M, Hayoune A, Hamana D (2004) J Mater Sci 39:1207. doi:10.1023/B:JMSC.0000013876.43031.67
45. Enzo S, Frattini R, Gupta R, Macri PP, Principi G, Schiffini L, Scipione G (1996) Acta Mater 44(8):3105
46. Amils X, Nogués J, Suriñach S, Muñoz JS, Lutterotti L, Gialanella S, Baró MD (1999) Nanostruct Mater 11:689